Exploring Mars at the nanoscale: Applications of transmission electron microscopy and atom probe tomography in planetary exploration

IOP Conf. Series: Materials Science and Engineering **891** (2020) 012008 doi:10.1088/1757-899X/891/1/012008

Exploring Mars at the nanoscale: Applications of transmission electron microscopy and atom probe tomography in planetary exploration

L Daly[1,4,5], M R Lee[1], P Bagot[2], J Halpin[3], W Smith[3], S McFadzean[3], A C O'Brien[1], S Griffin[1], L J Hallis[1] and B E Cohen[1]

[1] University of Glasgow, School of Geographical and Earth Sciences, Gregory Building, Glasgow G12 8QQ, Great Britain
[2] University of Oxford, Department of Materials, Oxford OX1 3PH, Great Britain
[3] University of Glasgow, School of Physics and Astronomy, Materials and Condensed Matter Physics, Glasgow G12 8QQ, Great Britain
[4] Curtin University, Space Science and Technology Centre, School of Earth and Planetary Sciences, GPO Box U1987, Perth, WA 6845, Australia
[5] University of Sydney, Australian Centre for Microscopy and Microanalysis, Sydney, 2006, NSW, Australia

E-mail: luke.daly@glasgow.ac.uk

Abstract. The upcoming Mars Sample Return (MSR) mission aims to deliver small quantities of Martian rocks to the Earth. Investigating these precious samples requires the development and application of techniques that can extract the greatest amount of high quality data from the minimum sample volume, thereby maximising science return from MSR. Atom probe tomography (APT) and transmission electron microscopy (TEM) are two complementary techniques that can obtain nanoscale structural, geochemical and, in the case of atom probe, isotopic information from small sample volumes. Here we describe how both techniques operate, as well as review recent developments in sample preparation protocols. We also outline how APT has been successfully applied to extraterrestrial materials in the recent past. Finally, we describe how we have studied Martian meteorites using TEM and APT in close coordination in order to characterise the products of water/rock interactions in the crust of Mars – a key science goal of MSR. Our results provide new insights into the Martian hydrosphere and the mechanisms of anhydrous-hydrous mineral replacement. In light of the unique results provided by these tools, APT and TEM should form a crucial part at the culmination of a correlative analytical pipeline for MSR mission materials.

1. Introduction

Rocks from Mars are among the rarest meteorites and are the only physical samples we currently have of the red planet. They represent a total of 277 individual stones, with a combined weight of 162.5031 kg [1] split between five main lithologies (four igneous and one breccia): the shergottites, nakhlites, chassignites, black beauty paired stone, and the anomalous Alan Hills (ALH) 84001 [1-4]. Cosmogenic exposure ages indicate that they sample 4 - 8 ejection sites on Mars [3]. A Mars sample return mission

is being planned to recover samples that had been previously collected and stored by the Mars 2020 rover; these samples will add a further ~ 0.5 kg of fresh oriented rocks to our collection - potentially including sedimentary lithologies [5, 6].

Martian meteorites have proven invaluable in providing insights into volcanic activity, the action of water and impact processes on Mars [2, 4, 7-11]. However, the rarity of Martian samples means that as analytical scientists we are duty bound to maximise the amount of data collected from the smallest sample volume to provide the greatest insight into Martian planetary processes. Here we describe our recent application of transmission electron microscopy (TEM) and atom probe tomography (APT) techniques to Martian meteorites. TEM and APT are two nanoscale techniques that provide the high-resolution culmination of a correlative analytical pipeline (Fig. 1) that maximises data output from the minimum sample volumes to address research questions pertinent to the red planet.

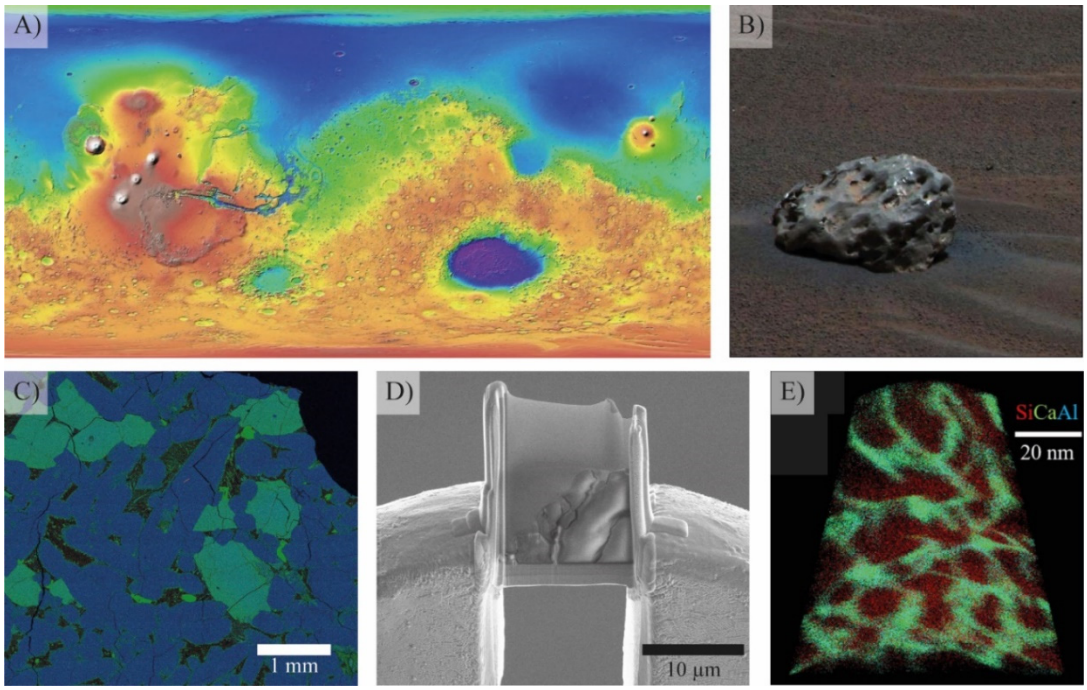

Figure 1. A correlative pipeline across a broad array of length scales to interpret the geological history the planet Mars. a) An elevation map of the Martian surface from the NASA MOLA science team. Image Credit: NASA/USGS Astrogeology Science Centre/Goddard Space Flight Centre. b) An image of an iron meteorite on the surface of Mars taken by NASA's Opportunity rover. Image credit NASA/JPL/Cornell. c) A red (Al), green (Fe), blue (Mg), EDS image of Martian meteorite Yamato 000802. d) A TEM lamella of a section through a magnetite grain in the Tissint meteorite. e) A APT analysis of an atom probe needle extracted from the mesostasis of Martian breccia Northwest Africa 11522 (after [12]).

2. Focussed ion beam TEM / APT sample preparation

The preparation of geological and extraterrestrial samples for TEM and APT usually involves extraction from a polished section using a focussed ion beam (FIB) instrument. Typical TEM sample preparation requires extracting a 1 - 2 µm thick bar of material that is then thinned to electron transparency, usually < 100 nm [13]. TEM samples produced by Ga-FIBs are generally 15 µm × 20 µm as larger samples would be too time intensive to extract. However, with the development of Xe/plasma-FIB

instrumentation that can remove 'vast' volumes of material rapidly, the width and depth of a TEM sample are limited only by the cohesive strength of the material. It is now feasible to produce 100 µm wide TEM sample. To avoid bending/warping during thinning of wider samples the structural integrity can be maintained by only thinning 'windows' at regular intervals, with structurally sound 'posts' in between. Wider TEM samples are no longer limited to small regions of interest and can now evaluate heterogeneities in mineralogy, density, porosity, etc., across 100 µm lengths. This is incredibly powerful in meteoritics because most meteorites are heterogeneous over these length scales.

Typical APT sample preparation approaches involve milling out a triangular prism and attaching segments to pre-prepared posts [14]. Sample mounts for APT are Cu or Mo five post grids otherwise used for TEM analysis that have been FIB milled into needles or pre-grown arrays of Si posts. Once attached, the APT samples are thinned using an annular milling pattern to produce a needle with a 100 nm diameter tip [14]. APT samples can also be prepared in situ using the 'satellite dish' method ([15] Fig. 2a). This approach involves cutting a 150 µm diameter wide 50 µm deep circular depression in the sample with APT needle in the centre [15]. A wedge shape 'window' is also cut to view the needle in the atom probe ([15] Fig. 2a). This approach maintains the orientation of the specimen relative to the sample. The satellite dish method combined with electron backscatter diffraction (EBSD) would be a powerful correlative analytical approach. However, this approach is only viable using a Xe-FIB due to the 'vast' amounts of material that need to be excavated and where most of the sample surrounding the region of interest is forfeit and as such is only suitable for specific applications. The 'button method' of FIB APT/TEM sample preparation enables sub-micrometre grains, interfaces, defects and twin boundaries to be targeted ([16] Fig. 2b). This approach becomes particularly powerful when combined with SEM, EBSD, FIB-TOF-SIMS characterisation prior to FIB preparation to pinpoint the region of interest [16]. A 'button' of electron beam deposited platinum is deposited to highlight the feature and locate it after covering with the ion beam protective Pt strip ([16] Fig. 2b). These buttons permit accurate extraction and thinning of TEM/APT samples to ensure the region of interest is contained within the sample. This approach has been successfully applied to extract 100 nm diameter refractory metal alloys in meteorites [17, 18].

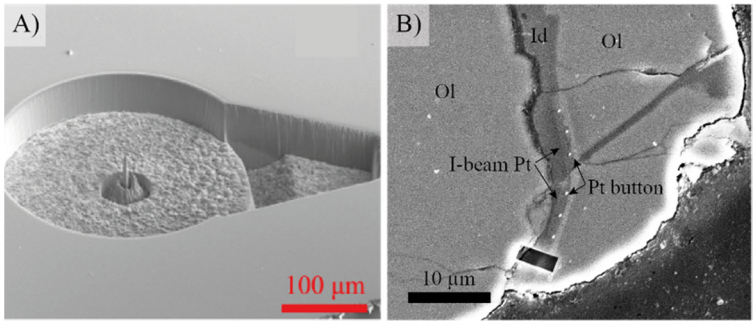

Figure 2. Images of a suite of FIB sample preparation approaches to both TEM and APT. a) APT sample preparation using the in situ 'satellite dish' approach, adapted from [15]. b) The 'button method' of APT sample preparation of dish from Rickard *et al.* [16] used here on to decorate and target the olivine-iddingsite interface in the Lafayette meteorite.

3. Transmission electron microscopy

TEM has been used extensively to characterise water-bearing minerals in Martian meteorites (e.g., [19, 20]), and is complementary to APT. TEM works by irradiating a thin sample – ideally < 100 nm – with a beam of high energy electrons (typically 200 kV) under vacuum. These thin samples are often referred to as 'electron transparent'. Those electrons that pass through the sample can be used to form images, down to atomic resolution. If the beam is relatively broad and static, bright- and dark-field images are formed using the unscattered and scattered electrons, respectively. By scanning a focussed beam over the sample, scanning TEM (STEM) images are formed, again in bright-field (using unscattered electrons) and dark-field (using scattered electrons) modes. Electron diffraction patterns

represent the angular range of scattering, and the *d*-spacings obtained from them can be used to identify minerals and determine their crystallographic orientation. The energy that the electrons lose as they pass through the sample can also be measured to obtain information on chemical composition and bonding (i.e., electron energy loss spectroscopy, EELS). An energy-dispersive X-ray spectrometer located above the thin sample enables quantitative and qualitative chemical analysis in the same manner as EDS in an SEM. For a more detailed description of TEM and STEM in planetary science see Lee [21].

4. Atom probe tomography

The APT technique is described in detail in Kelly and Larson [22] and Gault et al. [23]. Therefore, we only provide a brief overview of the technique here. APT is a high-resolution technique capable of analysing small cylindrical volumes (up to approximately 100 × 100 × 1,000 nm) with a spatial resolution of 0.3 nm in three dimensions [22]. The required specimen geometry for APT analysis is needle-like, with a 100 nm diameter tip and a half shank angle < 10° [22]. The needle-like specimen is loaded in the atom probe under high vacuum and situated near an annular electrode [24]. A voltage of ~ 1,000 V is applied to the specimen by the electrode. If the specimen is conductive, the voltage can be pulsed to facilitate field evaporation of individual atoms from the surface of the needle [22, 23]. However, if the sample is non-conductive (i.e., most geological and extraterrestrial samples) field evaporation can be initiated through the addition of heat by applying a high frequency (100 - 250 kHz) ultraviolet laser to the tip of the sample to achieve single atom ionisation [25]. It was the addition of the laser to atom probe instruments that enabled the analysis of non-conductive geological samples [25].

Field evaporated ions are accelerated across a potential difference where they impinge upon a position sensitive detector [22, 23]. The time of flight from laser/voltage pulse to impact provides the mass-to-charge-state-ratio of the ion and thus its elemental and isotopic identity, while the x- and y-coordinates on the detector can be used to reconstruct the initial position of the atom within the sample and thus reconstruct the 3D atomic structure of the sample [22, 23]. The detection efficiency of the detector is dependent on the available surface area on the detector surface, and is generally between 50 - 65 % [22, 23]. However, new generation detectors in atom probes have an increased surface area available for detection and can now collect over 80 % of the ions produced. In principle, the energy imparted to the sample should ionise all elements of the periodic table with equal efficiency resulting in 100 % ionisation of the sample [26, 27]. Therefore, APT does not, in theory, suffer mass dependant fractionation of isotopes or produce biases in the elements detected. The only sources of uncertainty are then derived from counting statistics based on the actual number of ions measured [25]. As such, APT has a high sensitivity and spatial resolution, and so can in principle be used to determine crystallography and atomic lattice spacings, complete geochemical characterisation including trace elements [18, 28-30], depict nanoscale geochemical heterogeneities and clustering of atoms [28, 31-33], and isotope analysis across all elements in the periodic table [34-39].

To extract elemental and isotope abundances from the mass-to-charge-state-ratio-spectrum resulting from the analysis, the total number of counts beneath each peak must be calculated. This is done by 'ranging' the counts beneath each peak [23] using the IVAS software package over a specific unified atomic mass unit (*u*) width followed by a local background subtraction from a nearby region that contains no peaks over the same *u* width. Details about ranging methods and advantages and disadvantages of different approaches can be found in Daly *et al.* [37] and Parman *et al.* [24]. In general, for geochemical analysis the full width of the peak should be used whereas for isotope analysis slightly less than the width of the smallest peak should be used consistently for all isotope peaks of interest [37].

Analysis of geological and extraterrestrial samples is complicated by the formation of multi-ion complexes, i.e., OH^+ or $Si_2O_3^+$. These result in isobaric interferences that need to be deconvolved to extract robust elemental or isotopic abundances. APT can detect trace abundances of elements down to 10 atomic parts per million (appm) for sample volumes over 106 nm^3 [22] while newer atom probe instruments are capable of detection limits as low as 1 appm. This means APT can be utilised to analyse

the trace element chemistry of mineral phases. Furthermore, the 3D reconstruction of the atomic positions and the size of the sample mean that it is possible to ensure only atoms emitted from the phase of interest are included in the spectrum. This means an accurate bulk chemistry of the phase of interest can be derived (e.g. [18, 28, 29, 40]). Therefore, APT is ideal for analysing sub-micrometre size phases whose trace element chemistry cannot be obtained through conventional techniques, or where the signal from the phase of interest is contaminated by contributions from surrounding phases. In addition, it is possible to extract nanostructural geochemical information such as planar or point cluster concentrations of elements even in trace amounts within samples. This approach has been demonstrated many times for the geochronological studies of Pb-clusters in zircon, and baddeleyite [31, 32, 34-36] and gold in arsenopyrite [28].

The mass resolving power ($m/\Delta m$), where m is mass and Δm is the variation in mass between atoms, of the atom probe is better than 1,000 [25, 41]. Therefore, APT is capable of discerning peaks separated by 0.15 *u* [25, 41]. Thus, isotopic peaks from ions of different charge states (i.e., $^{94}Mo^{3+}$ and $^{63}Cr^{2+}$) can be distinguished, but APT cannot currently determine the mass difference between ions that have the same mass (i.e., $^{54}Cr^{2+}$ and $^{54}Fe^{2+}$) [26, 42]. $^{54}Cr^{2+}$ and $^{54}Fe^{2+}$ have a difference in mass of 0:0005 *u*, which requires a mass resolving power > $1{:}5 \times 10^5$ [25, 41] to distinguish these ionic species. These isobaric interferences are beyond the mass resolving power of any technique currently available [25, 41] and require peak deconvolution to estimate the contribution of each isotope to the total peak. Field evaporation during APT analysis is ideal for isotopic analysis of nanoscale materials as the whole sample is ionised, and it is assumed that there is no bias in the detection of elements or between isotopes, i.e., all species are ionised and detected equally [26, 27]. However, unique factors in each analysis, such as voltage, tip shape and temperature are not constant between analyses and their effect on the resulting mass spectrum is not quantified and potentially not quantifiable [24, 32]. Despite these challenges a robust standardised approach for isotope analysis has been proposed for Re/Os isotope analysis and is readily adaptable to other isotope systems and can distinguish isotopic ratio variations between 0.5 – 1 % with substantial room for improvement [37].

5. A brief history of atom probe tomography in planetary science

The first paper on non-conductive geological materials using laser assisted atom probe microscopy was by Valley *et al.* [34] who demonstrated that the $^{207}Pb/^{206}Pb$ isotopic abundances can be measured in zircon using APT. The APT $^{207}Pb/^{206}Pb$ isotope ratio recorded an age consistent with measurements of the same zircon using secondary ion mass spectrometry (SIMS) [34]. This study put atom probe on the map as a powerful geochronological tool for geoscience applications that is capable of reliably reproducing results of other more established high precision isotopic techniques but using a much smaller sample volume.

One of the first uses of APT on extraterrestrial samples was Heck *et al.* [38] who reported APT data for C isotopic ratios in nanodiamonds within primitive chondritie meteorites. These results indicated that the $^{12}C/^{13}C$ ratio is anomalous relative to Solar System values [38]. However, these anomalous isotopic ratios may instead reflect contributions of ^{12}C-hydrides to the ^{13}C-peak [38] and possible underrepresentation of the ^{12}C-peak due to molecular ion formation and detector dead times [40]. This work has been followed by continued APT work on pre-solar grains in Lewis *et al.* [39], unpicking the nanostructures and geochronological information trapped in shocked zircon, baddeleyite, Lunar meteorites [33, 35, 36], and space weathered Lunar soil from the Apollo missions [42], unpicking the magnetic properties of iron meteorites [30], and geochemical analysis of refractory metal alloys [17, 18]. We have only scratched the surface of the insights of APT in planetary science.

The real interpretive power of APT and TEM is through correlative analysis combining several techniques to provide context to these nanoscale analyses (e.g., [16]). Below is an example workflow showing how light microscopy, SEM, EBSD, FIB, TEM, STEM and APT can be successfully combined to locate and characterise water-bearing minerals in Martian meteorites.

6. Water on Mars

Ashworth and Hutchison [7] first described evidence for water-bearing material in the nakhlite group of Martian meteorites (see [8] for a recent review). These authors described the water bearing material as "iddingsite", which they interpreted to have formed by hydrothermal alteration of olivine. This fluid that produced the iddingsite assemblage was oxidising in nature, low temperature (< 140 °C) [11] and affected these rocks approximately 633 Ma [43]. The heat source that melted these subsurface ices is not currently known, but the primary theories are impact generated hydrothermal activity [44] or a magmatic event [43].

The iddingsite veins can be readily identified using transmitted light microscopy (Fig. 3) and are a few micrometres in thickness. They resemble narrow veins of 'rust' in transmitted light (Fig. 4a) and although more detail can be observed by SEM (Figs. 4b and 4c) their properties remain difficult to determine. EDS shows that these veins have a Mg-Fe silicate composition (~ 40 wt% SiO_2, 40 wt% Fe_2O_3, 5 wt% MgO) and their low analytical totals (~ 85 - 90 wt%) indicate the presence of unanalysed OH/H_2O (i.e., Martian water). EBSD demonstrates that the veins have a preferred crystallographic orientation parallel to [010], and this crystallographic information can be used to help guide the orientation in which the electron-transparent samples can be cut and extracted using FIB (Figs. 2c and 2d). Bright-field TEM images show that the host olivine is microstructurally complex, probably reflecting mild shock metamorphism [20] whereas the iddingsite veins appear to be homogeneous and featureless (Fig. 4d).

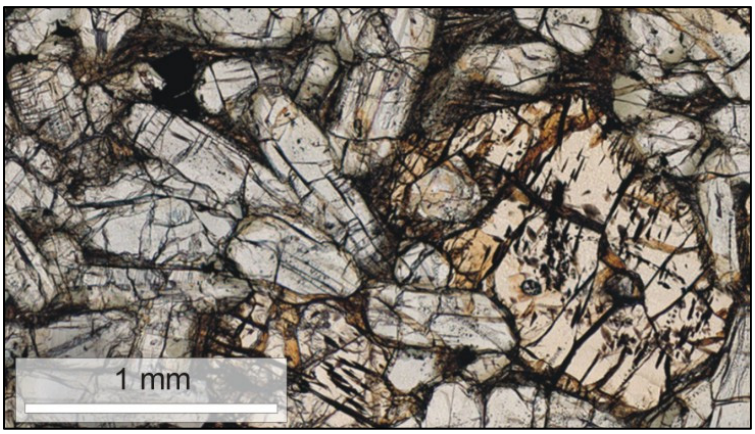

Figure 3. Transmitted light image of a thin section of the Nakhla meteorite. An olivine grain in the centre of the field of view has a light brown colour and is cut by several very thin veins of rust-coloured iddingsite. The clear tabular mineral grains are augite. Image from the Open University virtual microscope (www.virtualmicroscope.org/content/nakhla-2).

To characterise OH/H_2O-bearing Fe-Mg silicates, compositional maps were obtained from the area in Fig. 4d using EDS and EELS (Fig. 5). Results highlight the location of siderite and parts of the carbonate have altered to ferryhydrite ($Fe^{3+}_{8.2}O_{8.5}(OH)_{7.4} + 3H_2O$) (Fig. 5). As well as elemental analysis, EELS is used to determine the valence state of Fe (and other elements) [45]. An Fe valence map of the vein shows that the OH/H_2O-bearing Fe-Mg silicate and ferrihydrite both contain Fe^{3+}, whereas the siderite and olivine have Fe^{2+} as expected (Fig. 5).

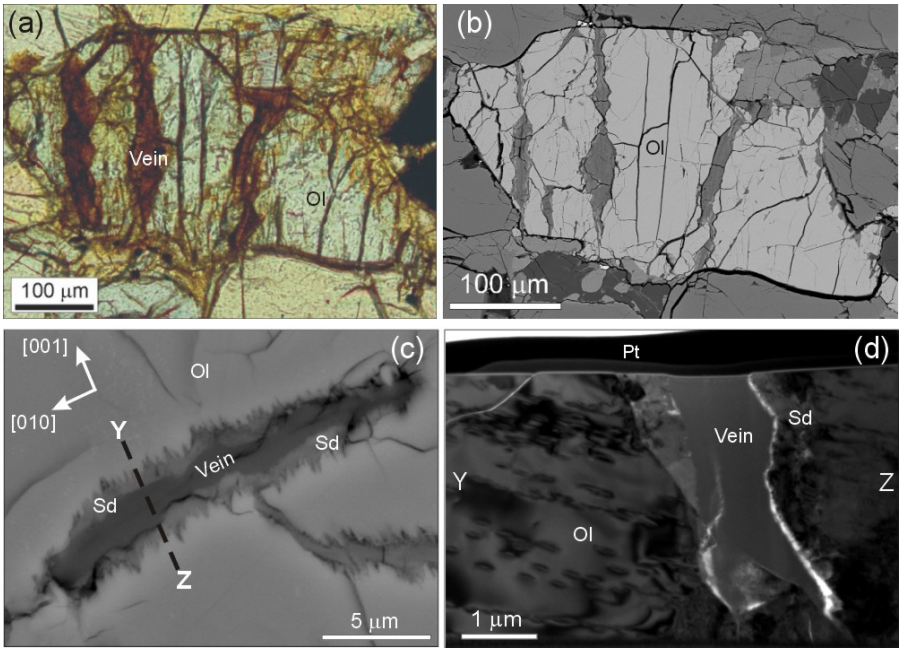

Figure 4. Iddingsite in the Lafayette meteorite, (a and b) [46], and the Nakhla meteorite (c and d) [20], hosted by olivine (Ol). a) Transmitted light image, and b) backscattered electron SEM image of an olivine grain that is cross-cut by three rust-brown coloured iddingsite veins. c) Backscattered electron SEM image of an iddingsite vein. Between the iddingsite and olivine is a selvage of siderite (Sd) with a finely serrated contact with olivine. The crystallographic orientation of the vein relative to the host olivine grain is indicated, as determined by EBSD. The dashed black line Y-Z denotes where a FIB-section was extracted. d) Bright-field TEM image of the sample extracted from (c). The olivine is various shades of grey as its defect-rich microstructure is diffracting electrons to different intensities. At this magnification the vein is homogeneous and apparently free of diffracting crystals. Siderite (Sd) is difficult to distinguish from olivine. The black band along the top of the image is the platinum (Pt) strap that was deposited by the FIB to protect the sample from ion beam damage.

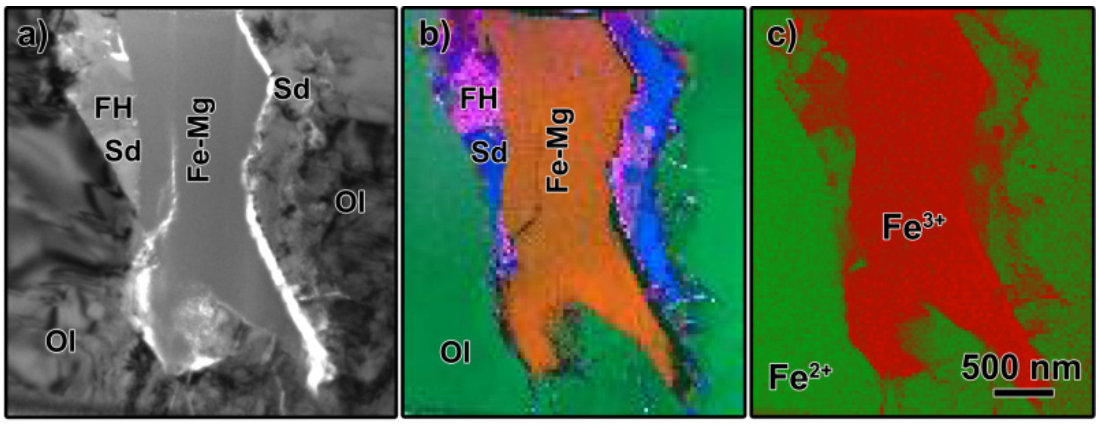

Figure 5. Iddingsite veins from the Nakhla meteorite (from [19], Fig. 3). a) Bright-field TEM image of a vein of OH/H_2O-bearing Fe-Mg silicate (Fe-Mg) that is flanked by siderite (Sd) and hosted by olivine (Ol). The siderite also contains ferrihydrite (FH). b) EDS map of (a) with element combinations coloured so as to render olivine green, siderite blue, ferrihydrite pink, and the Fe-Mg silicate orange. d) EELS valence map of (a) and (b) showing that olivine and siderite both contain Fe^{2+} (coloured green) and the Fe-Mg silicate and ferrihydrite have Fe^{3+} (red).

The identity of the OH/H_2O-bearing Fe^{3+}-Mg-silicate could not be determined by TEM imaging or EELS alone. Thus, higher resolution STEM images and EDS maps were obtained using an aberration-corrected TEM with a probe size of < 2 nm (Fig. 6). STEM images show that the Fe-Mg-silicate is composed of a closely packed mass of particles that are circular/oval and a few nanometres in diameter (Fig. 6a). EDS maps show that the particles are composed of Si and O with a Fe-rich rim (Fig. 6b). Given that this material contains OH/H_2O and its Fe^{3+}, the Fe-Mg-silicate is interpreted to be composed of nanoparticles of opaline silica (amorphous $SiO_2 \cdot nH_2O$) that are rimmed by Mg-bearing ferrihydrite.

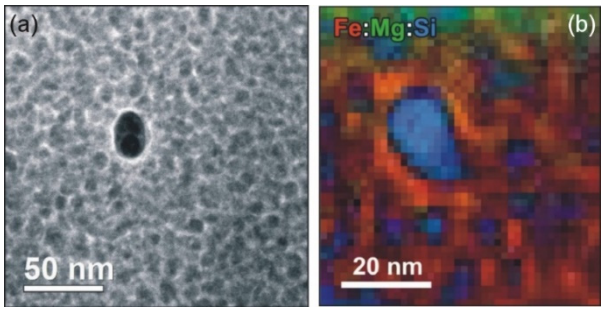

Figure 6. Iddingsite veins from the Nakhla meteorite (from [19] Fig. 4). a) High-angle annular dark-field (HAADF) image of the OH/H_2O-bearing Fe-Mg silicate showing that it is composed of a tightly packed mass of nanoparticles. b) EDS element map of one area of (a) demonstrating that the nanoparticles are composed of silica and have a Fe rich rim.

APT samples have been extracted across the nakhlite olivine-iddingsite interface (Fig. 7) to observe nanoscale geochemical gradients and corroborate TEM observations. APT analysis of iddingsite reveal it had a heterogeneous density consistent with the HAADF images obtained by TEM (Figs. 6a and 7) but homogeneous chemistry. As such on the length scales of an APT needle in this region, we only identified clay minerals. No oxides, carbonates, sulphates or halides [2] or nanoscale chemical domains were found. The density variations in iddingsite are interpreted to represent the preferential ionisation of individual phyllosilicate platelets (high density) followed by 'bursting' removing the clay mineral to leave a void (low density). APT analysis of across the iddingsite-olivine interface reveal that this boundary is gradational at the nanoscale. Towards the interface over 30 - 20 nm steady depletions in the major cations such as Mg are observed. These depletions are complemented by a steady enrichment in H towards the interface (Fig. 7). EBSD analysis of NWA 817 indicate the iddingsite vein is parallel to the (021) plane of the olivine consistent with previous petrographic descriptions of crystal orientation relationships in these meteorites [10]. However, the observation of a 20 nm wide diffuse boundary not a sharp boundary (Fig. 7) is inconsistent with recent models of fluid alteration of glasses, such as interfacial dissolution-reprecipitation [47]. Our APT data agree better with a diffusion coupled hydration model where inward diffusion of hydrogen species is coupled with outward diffusion of cations [48]. In addition, this 20 nm layer may store H more securely than iddingsite whose hydrogen isotopic composition is strongly perturbed by terrestrial weathering [49, 50] making inferences about the fluids origin challenging. However, directly measuring the D/H ratio of hydrogen contained within the olivine across these interfaces may reveal the D/H ratio of the original fluid, and thereby constrain its source (e.g., Martian crust versus atmosphere).

7 Conclusion

We stand upon the edge of a nanorevolution in planetary science. Through measurements at the atomic-scale using TEM and APT we can provide new insights into Martian and Solar System processes that act on length scales over 20 orders of magnitude larger than the sample volume analysed such as action of water on Mars that has implications for past and future habitability of the red planet. APT combined with improvements to the resolution of more traditional analytical approaches like TEM is about to open a whole new suite of nanoscale observations. This is particularly important for samples from the

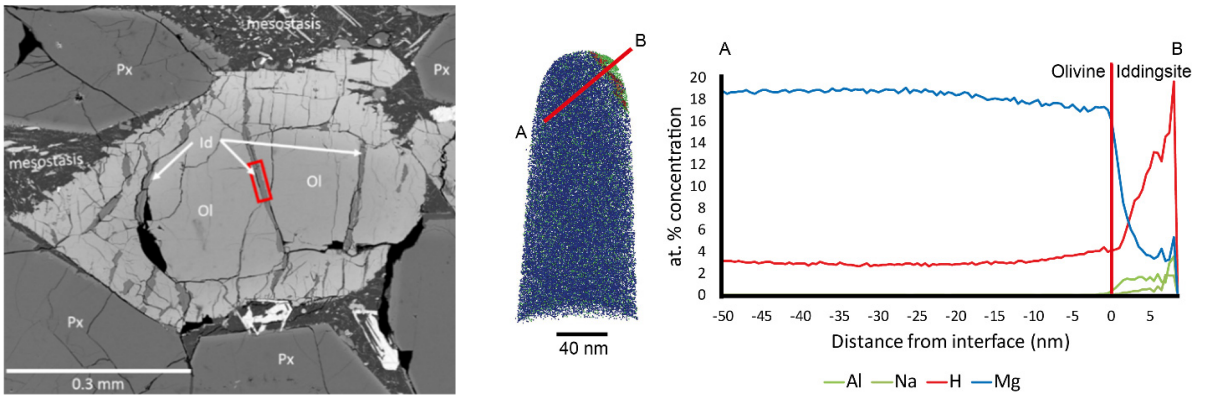

Figure 7. APT analysis of an olivine-iddingsite interface in nakhlite meteorite NWA 817. Image to the left is a backscattered electron (BSE) image of an olivine phenocryst with cross-cutting crystallographically controlled iddingsite veins. A set of APT samples were extracted from the red box so as the iddingsite-olivine interface was present at the apex of the needle. Ol = Olivine, Id = Iddingsite, Px = Pyroxene. Image below is an APT analysis across an olivine-iddingsite interface. The atom map represented by Mg (blue dots) and Na (green dots) atoms defines the interface (red iso-concentration surface). The graph shows a concentration profile of the major elements across the boundary from iddingsite (b) into olivine (A) where a clear depletion of Mg and enrichment of hydrogen is observed up to 20 nm into the olivine. The origin of the majority of the hydrogen signal within APT dataset is likely a combination between inherent hydrogen in the sample and background hydrogen from the sample chamber that is currently challenging to distinguish. However, recent deuteration experiments have shown a clear pathway to conduct these studies in the future [51-53]. In particular, deuteration experiments conducted on olivine by [53] indicate that variations in hydrogen at grain surfaces and reaction interfaces, similar to those detected here are real variations inherent in the sample and as such may provide a secure reservoir for Martian hydrogen. Image after [54].

red planet where meteorite samples are rare and the planned Mars sample return mission will provide at most a kilogram of material. Therefore, it is critical to maximise the research output from these small sample volumes. The combination of APT and TEM form a final set of techniques at the end of a correlated pipeline of analysis that will maximise the information gathered from such small sample volumes.

Acknowledgements
The authors would like to thank proceedings editors as well as one anonymous reviewer for their valuable comments that improved this manuscript. This work was funded by STFC, grant number ST/T002328/1 to MRL.

References
[1] Meteoritical Bulletin Database. 2019 Martian meteorites
[2] Agee C B, *et al.* 2013 Unique meteorite from early Amazonian Mars: Water-rich basaltic breccia Northwest Africa 7034. *Science* **339** 780-785
[3] Nyquist L, *et al.* 2001 Ages and geologic histories of Martian meteorites. in: *Chronology and evolution of Mars*. (New York, NY: Springer) 105-164
[4] McSween H Y 2015 Petrology on Mars. *Amer. Mineralogist* **100** 2380-2395
[5] Williford K H, *et al.* 2018 The NASA Mars 2020 rover mission and the search for extraterrestrial life. in: *From habitability to life on Mars*. (Amsterdam, The Netherlands: Elsevier) 275-308

[6] iMOST, *et al.* 2018 *The potential science and engineering value of samples delivered to Earth by Mars Sample Return.* Mars Exploration Program Analysis Group (MEPAG). White paper, 186.
[7] Ashworth J and Hutchison R 1975 Water in non-carbonaceous stony meteorites. *Nature* **256** 714-715
[8] Cohen B 2017 Taking the pulse of Mars via 40Ar/39Ar dating of a plume-fed volcano. *Nature Comm.* **8** 640
[9] Harvey R P and McSween H Y 1992 Petrogenesis of the nakhlite meteorites: Evidence from cumulate mineral zoning. *Geochim. Cosmochim. Acta*, **56** 1655-1663
[10] Treiman A H 2005 The nakhlite meteorites: Augite-rich igneous rocks from Mars. *Chemie der Erde-Geochemistry* **65** 203-270
[11] Bunch T and Reid A M 1975 The nakhlites Part I: Petrography and mineral chemistry. *Meteoritics Planet. Sci.* **10** 303-315
[12] Daly L, *et al.* 2018 High pressure excursions in the matrix of Martian meteorite North West Africa (NWA) 11522. in: *81st Ann. Meeting of the Meteoritical Society* 2067
[13] Lee M, Bland P and Graham G 2003 Preparation of TEM samples by focused ion beam (FIB) techniques: applications to the study of clays and phyllosilicates in meteorites. *Mineral. Mag.* **67** 581-592
[14] Thompson K, *et al.* 2007 In situ site-specific specimen preparation for atom probe tomography. *Ultramicroscopy* **107** 131-139
[15] Halpin J E, *et al.* 2019 An in-situ approach for preparing atom probe tomography specimens by xenon plasma focused ion beam milling. *Ultramicroscopy* **202** 121-127
[16] Rickard W, *et al.* 2020 Novel Applications of FIB-based ToF-SIMS in Atom Probe Tomography Workflows. *Microsc. Microanal.* doi.org/10.1017/S1431927620000136
[17] Daly L, *et al.* 2017 Crystallography of refractory metal nuggets in carbonaceous chondrites: A transmission Kikuchi diffraction approach. *Geochim. Cosmochim. Acta* **216** 42-60
[18] Daly L, *et al.* 2017 Nebula sulfidation and evidence for migration of "free-floating" refractory metal nuggets revealed by atom probe microscopy. *Geology* **45** 847-850
[19] Lee M, *et al.* 2015 Opal-A in the Nakhla meteorite: A tracer of ephemeral liquid water in the Amazonian crust of Mars. *Meteoritics Planet. Sci.* **50** 1362-1377
[20] Lee M, *et al.* 2013 Evidence for silicate dissolution on Mars from the Nakhla meteorite. *Meteoritics Planet. Sci.* **48** 224-240
[21] Lee M 2010 Transmission electron microscopy (TEM) of Earth and planetary materials: A review. *Mineral. Mag.* **74** 1-27
[22] Kelly T F and Larson D J 2012 Atom probe tomography 2012. *Ann. Rev. Mater. Res.* **42** 1-31
[23] Gault B, *et al.* 2012 *Atom probe microscopy, vol. 160*. (New York, NY: Springer Science and Business Media)
[24] Parman S W, *et al.* 2015 Atom probe tomography of isoferroplatinum. *Amer. Mineralogist* **100** 852-860
[25] Larson D J, *et al.* 2013 *Local electrode atom probe tomography*. (New York, NY: Springer Science)
[26] Kingham D R 1982 The post-ionization of field evaporated ions: A theoretical explanation of multiple charge states. *Surface Sci.* **116** 273-301
[27] Straub H, *et al.* 1999 Absolute detection efficiency of a microchannel plate detector for kilo-electron volt energy ions. *Rev. Sci. Instrum.* **70** 4238-4240
[28] Fougerouse D, *et al.* 2016 Nanoscale gold clusters in arsenopyrite controlled by growth rate not concentration: Evidence from atom probe microscopy. *Amer. Mineralogist* **101** 1916-1919
[29] Pérez-Huerta A, *et al.* 2016 Atom probe tomography (APT) of carbonate minerals. *Micron* **80** 83-89
[30] Einsle J F, et al. 2018 Nanomagnetic properties of the meteorite cloudy zone. *Proc. Nat. Acad. Sci.* **115** E11436-E11445

[31] Piazolo S, *et al.* 2016 Deformation-induced trace element redistribution in zircon revealed using atom probe tomography. *Nature Comm.* **7** 10490
[32] Reddy S M, *et al.* 2016 Mechanisms of deformation-induced trace element migration in zircon resolved by atom probe and correlative microscopy. *Geochim. Cosmochim. Acta* **195** 158-170
[33] Montalvo S D, *et al.* 2019 Nanoscale constraints on the shock-induced transformation of zircon to reidite. *Chem. Geol.* **507** 85-95
[34] Valley J W, *et al.* 2014 Hadean age for a post-magma-ocean zircon confirmed by atom-probe tomography. *Nature Geosci.* **7** 219-223
[35] White L, *et al.* 2017 Atomic-scale age resolution of planetary events. *Nature Comm.* **8** 15597
[36] White L F, *et al.* 2019 Crystallization and impact history of a meteoritic sample of early lunar crust (NWA 3163) refined by atom probe geochronology. *Geosci. Frontiers* **10** 1841-1848
[37] Daly L, *et al.* 2018 Defining the potential of nanoscale Re-Os isotope systematics using atom probe microscopy. *Geostand. Geoanal. Res.* **42** 279-299
[38] Heck P R, *et al.* 2014 Atom-probe analyses of nanodiamonds from Allende. *Meteoritics Planet. Sci.* **49** 453-467
[39] Lewis J, *et al.* 2015 Atom-probe tomography measurements of isotopic ratios of high-field materials with corrections and standardization: A case study of the 12C/13C of meteoritic nanodiamonds. *Microsc. Microanal.* **21** (Suppl. 3) 39-40
[40] Thuvander M, *et al.* 2011 Quantitative atom probe analysis of carbides. *Ultramicroscopy* **111** 604-608
[41] Kelly T F 2011 Kinetic-energy discrimination for atom probe tomography. *Microsc. Microanal.* **17** 1-14
[42] Goupon P, *et al.* 2017 Ultra-reduced pases in Apollo 16 regolith: Combined field emission electron probe microanalysis and atom probe tomography of submicron Fe-Si grains in Apollo 16 sample 61500. *Meteritics Planet. Sci.* **52** 9 1941-1962
[43] Borg L and Drake M J 2005 A review of meteorite evidence for the timing of magmatism and of surface or near-surface liquid water on Mars. *J. Geophys. Res.: Planets* **110** E12S03
[44] Osinski G R, *et al.* 2013 Impact-generated hydrothermal systems on Earth and Mars. *Icarus* **224** 347-363
[45] Garvie L A and Buseck P R 1998 Ratios of ferrous to ferric iron from nanometre-sized areas in minerals. *Nature* **396** 667
[46] Lee, M R, *et al.* 2015 Formation of iddingsite veins in the martian crust by centripetal replacement of olivine: Evidence from the nakhlite meteorite Lafayette. *Geochim. Cosmochim. Acta* **154** 49-65.
[47] Hellmann R, *et al.* 2015 Nanometre-scale evidence for interfacial dissolution–reprecipitation control of silicate glass corrosion. *Nature Mater.* **14** 307
[48] Grambow B 2006 Nuclear waste glasses - How durable? *Elements* **2** 357-364
[49] Lee M R, *et al.* 2018 Aqueous alteration of the Martian meteorite Northwest Africa 817: Probing fluid–rock interaction at the nakhlite launch site. *Meteoritics Planet. Sci.* **53** 2395-2412
[50] Hallis L, *et al.* 2012 Hydrogen isotope analyses of alteration phases in the nakhlite martian meteorites. *Geochim. Cosmochim. Acta* **97** 105-119
[51] Sundell G, *et al.* 2015 Direct observation of hydrogen and deuterium in oxide grain boundaries in corroded zirconium alloys. *Corrosion Sci.* **90** 1-4
[52] Chen Y S, *et al.* 2017 Direct observation of individual hydrogen atoms at trapping sites in a ferritic steel. *Science* **355** 1196-1199
[53] Daly L, *et al.* 2019 Solar wind hydration of Itokawa olivine. in: *82nd Ann. Meeting of the Meteoritical Society* 6273
[54] Daly L, *et al.* 2018 Insights into Martian fluid-rock reactions by atom probe tomography of the interface between nakhlite olivine and iddingsite. in: *50th Lunar and Planetary Science Conference* **50** 2132